

Searches for dark matter and new physics with unconventional signatures

C.-E. WULZ, on behalf of the CMS COLLABORATION

Institute of High Energy Physics of the Austrian Academy of Sciences - Vienna, Austria

received 26 July 2016

Summary. — Selected results on searches for dark matter and unconventional signatures with the CMS detector are presented. Dark matter searches in channels with one or two jets, single photons, vector bosons, or top and bottom quarks combined with missing momentum in the final states are described. Unusual signatures such as displaced objects, disappearing or kinked tracks, delayed or stopped particles have also been explored. The analyses were performed with proton-proton data recorded at LHC centre-of-mass energies up to 13 TeV.

1. – Introduction

After finding the Higgs boson in 2012, physics beyond the standard model is now the primary research topic at the Large Hadron Collider (LHC). Extensions of the standard model predict additional Higgs bosons and a wealth of other exotic particles. Searches for new phenomena, however, have been inconclusive so far. The recent increase of the LHC's centre-of-mass energy from 8 to 13 TeV has opened up new areas of phase space to find or to exclude new particles. In this report we concentrate on dark matter and unconventional signatures. Dark matter searches in channels with one or two jets, single photons, vector bosons, or top and bottom quarks combined with missing momentum in the final states are described. Unusual signatures such as displaced objects, disappearing or kinked tracks, delayed or stopped particles have also been explored. Results from proton-proton data recorded with the CMS experiment [1] at LHC centre-of-mass energies of 7, 8 and 13 TeV are presented. An overview of relevant current beyond-the-standard-model physics studies is available on dedicated web pages [2], in particular under “Exotica” and “Beyond 2 Generations”.

2. – Dark matter

One of today's biggest puzzles is the nature of dark matter. Beside axions, weakly interacting massive particles (WIMP) are well-motivated candidates. A large range of

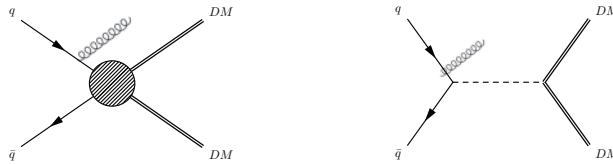


Fig. 1. – Feynman diagrams for the pair production of dark matter particles for the case of a contact interaction (left) and the exchange of a mediator (right).

experiments is currently searching for them in space, at underground facilities, or at accelerators. Direct detection is based on the scattering of WIMP dark matter off atomic nuclei, whereas indirect detection makes use of secondary radiation emitted in their pair annihilation. Experiments such as LUX, XENON, CDMS or CRESST belong to the first category, and space probes such as AMS02, PAMELA, FERMI or the IceCube observatory at the South Pole belong to the latter. At the LHC one can search for dark matter particles emerging in collisions of protons, recorded at the general-purpose experiments ATLAS and CMS. The methods are based on the detection of particles produced in association with the dark matter. They are complementary to the ones used in direct or indirect searches and are particularly well suited to low-mass WIMPs and spin-dependent interactions. Two scenarios for producing dark matter particles (DM, χ) can be envisaged, depending whether a contact interaction within an effective field theory approach is appropriate or whether a mediator between ordinary and dark matter comes into a mass range where it could be accessible at the LHC, as depicted in fig. 1. Since dark matter is assumed to interact very weakly with standard model particles it can only be detected indirectly, through an imbalance of the total momentum of all particles reconstructed in the plane transverse to the LHC beams. Its magnitude is denoted as missing transverse energy or E_T^{miss} . We focus on the search in the so-called mono- X channels, where objects X are accompanied by E_T^{miss} . X stands for quarks, gluons, W , Z , t , b , $t\bar{t}$, or $b\bar{b}$.

In the mono-jet search [3] the CMS event selection requires either $E_T^{\text{miss}} > 120$ GeV calculated from calorimeter information, or a jet reconstructed with the particle-flow technique [4, 5] with transverse momentum $p_T > 80$ GeV, and $E_T^{\text{miss}} > 105$ GeV, where E_T^{miss} is also reconstructed with the particle-flow algorithm, but excludes muons. As signal events typically contain jets from initial-state radiation, a second jet is allowed only if its distance in azimuth from the jet with the highest p_T is within 2.5 radians, thus suppressing the di-jet QCD background. Events with more than two jets with $p_T > 30$ GeV and pseudorapidity $|\eta| < 4.5$ are discarded, thereby significantly reducing backgrounds from $t\bar{t}$ and multi-jet events. The dominant backgrounds come from $Z(\rightarrow \nu\nu) + \text{jets}$ and $W(\rightarrow \ell\nu) + \text{jets}$ events, and are estimated from data samples of $Z(\rightarrow \mu\mu)$ and $W(\rightarrow \mu\nu)$ events, respectively. We studied scalar, vector, axial-vector and tensor interactions for a Dirac DM particle. Figure 2 (left) shows CMS upper limits for the DM-nucleon cross sections for spin-independent couplings as a function of the mass M_χ , derived from the mono-jet search. Curves from other experiments are overlaid, as well as an area with a possible signal seen by CDMS [6]. A similar plot for spin-dependent interactions is shown in fig. 2 (centre). Should an effective theory not be valid at LHC energies, we considered the case of an s -channel mediator with vector interactions. The resonant enhancement in the production cross section, once the mass of the mediator

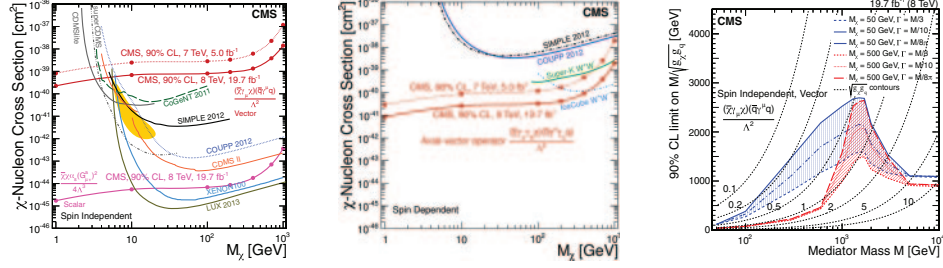


Fig. 2. – Upper limits on the χ -nucleon cross section, at 90% confidence level, plotted against the dark matter particle mass and compared with previous results, for spin-independent interactions in the mono-jet channel (left), and for spin-dependent interactions also in the mono-jet channel (centre); observed limits on $M/\sqrt{g_\chi g_q}$, the mediator mass divided by roots of DM and quark couplings, obtained from the mono-jet analysis (right).

(M) is within the kinematic range and can be produced on-shell, can be clearly seen in fig. 2 (right), which shows results for two dark matter masses and different mediator widths Γ .

A new mono-jet-channel analysis has been performed at $\sqrt{s} = 13$ TeV [7]. Two types of simplified models were considered, one with a spin-0 and the other with a spin-1 mediator. The analysis differs from the previous one in that new electron control regions have been added and the single lepton control regions are used to predict both the W and the Z boson backgrounds. The DM signal is extracted by a fit to the E_T^{miss} distribution as can be seen in fig. 3 (left). In fig. 3 (centre) one can see that the cross section limits as a function of the DM mass established by LUX are most sensitive down to 6 GeV, whereas the CMS limits are very competitive at lower masses. Comparisons of the 8 and 13 TeV DM mass reach as a function of the mediator mass are shown in fig. 3 (right). The excluded region is to the bottom-left of the contours shown in all cases except for that from the relic density as indicated by the shading. Mediator masses ranging up to 1.3 TeV are excluded at 90% confidence level (CL). Given the much smaller dataset, the exclusion limits are less stringent than the current best bounds from the 8 TeV studies, which reach up to 1.6 TeV of vector mediator mass.

An innovative DM search using the razor technique in the di-jet channel has also been performed, which sheds light on the range of validity of effective field theories [8]. Razor

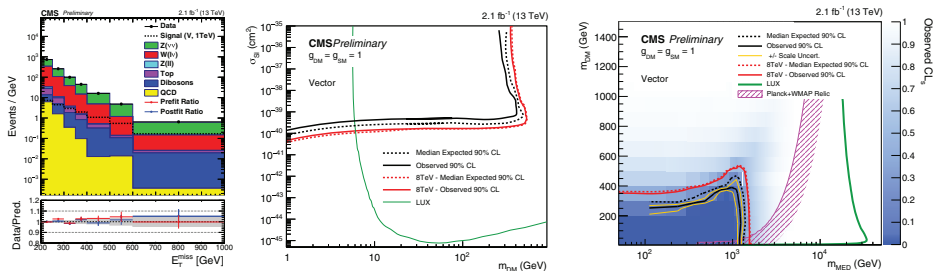


Fig. 3. – Missing momentum distribution (left), cross section limits (centre), and DM mass reach for vector interactions (right).

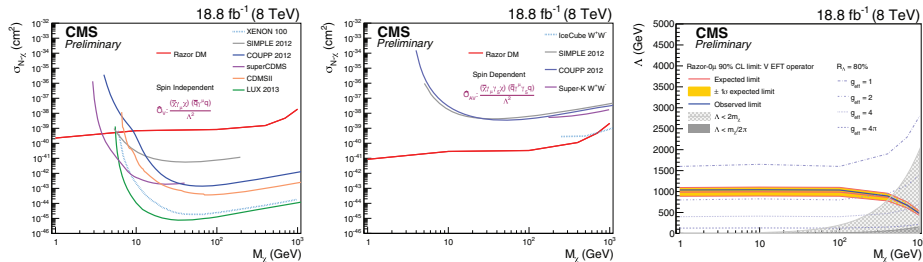


Fig. 4. – Upper limits at 90% confidence level on the DM-nucleon scattering cross section as a function of the DM mass in the case of spin-independent vector- (left) and spin-dependent axial-vector currents (centre); lower limits at 90% CL on the cutoff scale Λ as a function of the DM mass in the case of vector currents (right). The validity of the effective field theory for different values of the effective coupling g_{eff} is quantified by $R_\Lambda = 80\%$ contours.

variables, computed from the jet transverse momenta and E_T^{miss} , quantify the balance of the jet momenta. They have been developed in particular to suppress backgrounds from QCD. It has been shown that these variables are also sensitive to direct DM production [9]. The di-jet event topology provides a good discrimination against standard model backgrounds with looser event selection criteria than those used in the mono-jet searches. This fact compensates for the reduction in signal cross section due to the requirement of more jets in the final state. The net result is a sensitivity comparable to that of mono-jet searches. Figure 4 shows spin-independent (left) and spin-dependent (centre) upper limits on the DM-nucleon scattering cross section obtained with the di-jet razor analysis, together with results from other experiments. As mentioned before, the DM production below a cut-off energy scale Λ can be described as a contact interaction between two quarks and two DM particles. In the case of the s -channel production through a heavy mediator, Λ is identified with M/g_{eff} , where $g_{\text{eff}} = \sqrt{g_\chi g_q}$ is an effective coupling, determined by the couplings of the mediator to quark and DM fields. Lower limits on the cut-off scale are shown in fig. 4 (right). Following studies presented in refs. [10–12], we use the variable R_Λ to quantify the fraction of events for which an effective field theory hypothesis is still valid. R_Λ is computed as a function of the effective coupling g_{eff} in the range $0 < g_{\text{eff}} < 4\pi$. The contours corresponding to $R_\Lambda = 80\%$ for different values of g_{eff} are also outlined in fig. 4 (right). For values of $g_{\text{eff}} \gtrsim 2$, the limits set by the analysis lie above the $R_\Lambda = 80\%$ contours.

Other searches for DM have been performed in the mono-photon [13], mono-Z [14] and mono-W [14] channels. The top plots of fig. 5 show DM-nucleon cross section limits for vector and axial-vector interactions obtained in the mono-photon channel, together with results from other channels and other experiments. Similar spin-independent results for the mono-Z channel are depicted in fig. 5 (bottom left), which also shows results from the CMS invisible Higgs analysis, in addition to curves from direct detection experiments. The annihilation rate of Dirac fermion DM is ruled out at 90% CL for $m_\chi < 7$ GeV in case of vector coupling and $m_\chi < 32$ GeV in case of axial-vector coupling, as can be seen from fig. 5 (bottom right).

A DM interpretation of a previous W' analysis [15] has been performed, making use of the advantages that the standard model background is lower than in mono-jet or mono-photon channels, and that there is a lepton available to trigger on. The event selection required a prompt or non-prompt single electron or muon plus missing momentum.

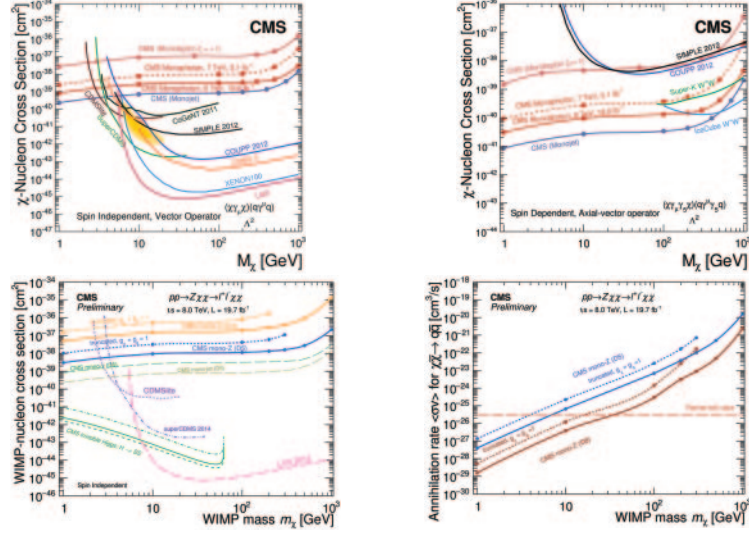


Fig. 5. – DM-nucleon cross section limits for the mono-photon channel for vector interactions (top left) and axial-vector interactions for the mono-Z channel (top right); DM-nucleon cross section limits for spin-independent interactions for the mono-Z channel (bottom left). D5 and C3 denote specific spin-independent vector and scalar operators, respectively; Annihilation rate for DM to quark pairs obtained from the mono-Z channel (bottom right).

The non-prompt leptons can come from τ decays. Interference has been taken into account, since the relative coupling strengths λ_u, λ_d to DM could be different for up- and down-type quarks. Figure 6 (left) shows DM-proton cross section limits for axial-vector interactions and three interference scenarios, with $\xi = \lambda_u \lambda_d$. Figure 6 (right) shows the DM production cross section multiplied by the branching fraction for the mono-W channel. The excluded cross section is flat as a function of M_χ , as expected since the signal kinematics do not change appreciably for different M_χ . For high M_χ the phase space to produce two heavy particles and a W boson is small, therefore the signal cross section is reduced and its shape more consistent with the background.

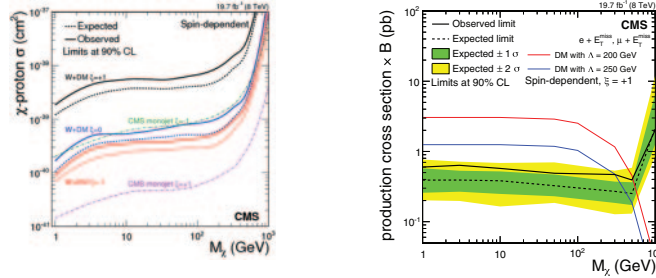


Fig. 6. – Excluded proton–dark-matter cross section for axial-vector couplings, for the combination of the electron and muon channels. For comparison, the result from the mono-jet DM search is also shown (left); upper limits on $\sigma \times \mathcal{B}(pp \rightarrow \chi\chi\ell\nu)$ for axial-vector couplings for the case $\xi = +1$ (right).

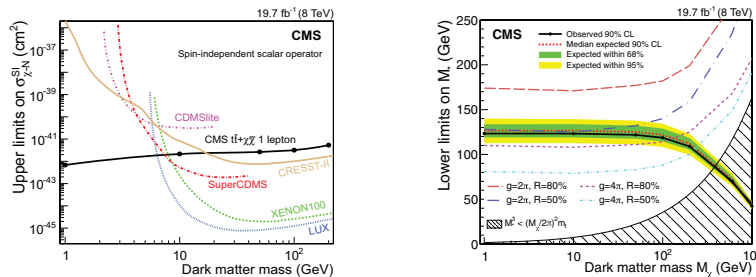


Fig. 7. – The 90% CL upper limits on the DM-nucleon spin-independent scattering cross sections as a function of the DM particle mass for scalar interactions. Also shown are limits from various direct DM search experiments (left); Observed exclusion limits in the plane of DM particle mass and interaction scale, with the region below the solid curve excluded at a 90% CL (right).

Quark-DM couplings for heavy flavours may be enhanced in scalar interactions. Searches have therefore been performed in channels with top pairs [16] and one or two b quarks [17], the latter already at $\sqrt{s} = 13$ TeV. For the $t\bar{t}$ plus E_T^{miss} channel the event selection required a single lepton accompanied by jets, at least one of which has a b tag. In fig. 7 (left) one can see the upper limit on the DM-nucleon cross section in this channel, together with comparisons from other experiments. Interpreting the findings in the context of a scalar interaction between dark matter particles and top quarks in the framework of an effective field theory, lower limits on the interaction scale are set. Assuming a dark matter particle with a mass of 100 GeV, values of the interaction scale below 118 GeV are excluded at 90% CL, which is shown in fig. 7 (right). A lower bound of the validity of the effective field theory is indicated by the upper edge of the hatched area. The four curves, corresponding to different g and R values, represent the lower bound on M^* for which 50% and 80% of signal events have a pair of DM particles with an invariant mass less than $g\sqrt{M^{*3}/m_t}$, where $g = 4\pi$ and $g = 2\pi$ respectively. These curves indicate further restrictions on the applicability of effective field theories. Figure 8 shows results from the first DM search at 13 TeV in the b quark channel. Events with one or two b jets in association with E_T^{miss} were selected. The analysis is also sensitive to DM production processes in association with t quarks decaying to b's. In fig. 8 (right) one can see that mediator-DM couplings up to $5 \times \sigma/\sigma_{g_{\chi=1}}$ are excluded.

3. – Unconventional signatures

Long-lived particles are predicted in many beyond-standard-model theories such as in gauge- or anomaly-mediated supersymmetry (SUSY) breaking scenarios, in R -parity violating SUSY and split SUSY models, or in hidden valley scenarios implying a dark sector. They could give rise to unusual signatures, which could imply displaced objects, disappearing or kinked tracks, and delayed objects. Displaced objects would manifest themselves through their origin from a vertex displaced by $O(10)$ mm from the primary vertex. Disappearing or kinked tracks would appear after a flight distance of $O(100)$ mm. Delayed objects refer to very long-lived or stable particles, which penetrate the detector and have decay lengths in excess of $O(1)$ m. We focus on neutral particles decaying to muons at 8 TeV [18], and on a first search for heavy charged particles at 13 TeV [19]. A search for stopped particles at 8 TeV is also described [20]. Two models have been considered in a study of long-lived particles decaying to muons, with a topology requiring

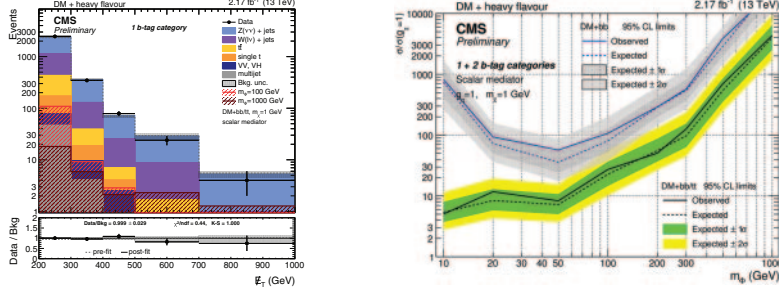


Fig. 8. – Observed and expected number of events in the single b-tag category (left); Observed exclusion limit, and expected limit with 1σ and 2σ uncertainty bands, for the 1 and 2 b-tag categories as a function of the mass of the scalar mediator. The DM candidate is assumed to have a mass equal to 1 GeV (right).

two muons originating from a displaced vertex, detected in the muon chambers only and not in the inner tracker of CMS. The muon reconstruction and selection efficiencies evaluated by Monte Carlo simulations have been cross-checked with cosmic data. Limits have been derived for a non-standard-model Higgs boson H decaying to two long-lived spin-0 bosons X , and for a squark pair, where each squark decays to a quark and a long-lived neutralino, which in turn decays to two muons and a neutrino in an R -parity-violating scenario. The study is orthogonal to a previous one that used only the tracker [21]. It improves sensitivity to particles that are particularly long-lived. The two analyses have been combined. The example plots of fig. 9 show upper limits on the cross sections multiplied by the branching fractions into two muons for the long-lived particles in the two models, with various combinations of masses for X bosons and squark/neutralino mass ratios.

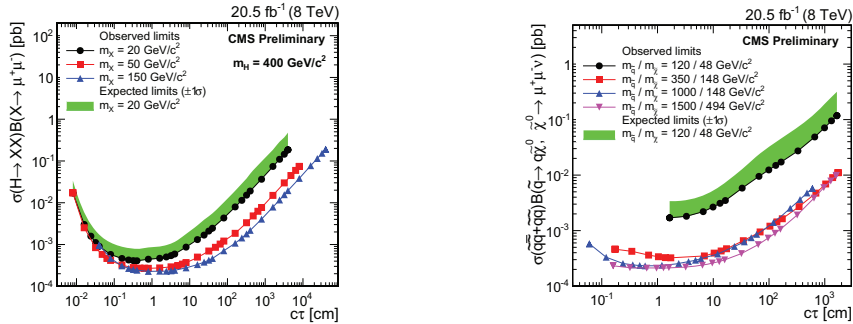


Fig. 9. – 95% CL upper limits on $\sigma(H \rightarrow XX) \mathcal{B}(X \rightarrow \mu^+ \mu^-)$ for $m_H = 400$ GeV with various X mass points (left). The shaded band shows the $\pm 1\sigma$ range of variation of the expected limits for the case of a 20 GeV X boson mass. Corresponding bands for the other X boson masses show a similar level of agreement and are omitted for clarity; 95% CL upper limits on $\sigma(q\bar{q} + q\bar{q}) \mathcal{B}(q \rightarrow q\tilde{\chi}^0, \tilde{\chi}^0 \rightarrow \mu\mu\nu)$ as a function of the neutralino lifetime. Shaded bands show the $\pm 1\sigma$ range of variation of the expected limits for the case of a 120 GeV squark and a 48 GeV neutralino mass. Corresponding bands for the other squark and neutralino masses show a similar level of agreement and are omitted for clarity.

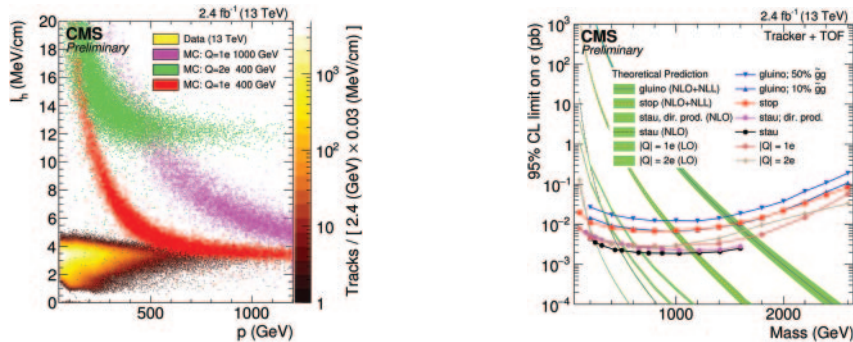


Fig. 10. – Distribution of the dE/dx estimator I_h versus particle momentum for data and simulations of singly or multiply charged particles (left); cross section upper limits at 95% CL for various signal models (right).

Long-lived heavy charged particles were searched for by requiring an anomalously high energy deposit in the tracker and a long time-of-flight to the muon detectors. From fig. 10 (left), which shows the harmonic estimator I_h for dE/dx and the expected number of tracks for data and Monte Carlo estimations for singly and doubly charged particles of different masses, no signal has been found. From fig. 10 (right) a lower mass limit for gluinos of 1590 GeV can be deduced, which is the most stringent limit to date.

REFERENCES

- [1] CMS COLLABORATION, *JINST*, **3** (2008) S08004.
- [2] <http://cms-results.web.cern.ch/cms-results/public-results/publications/>.
- [3] CMS COLLABORATION, *Eur. Phys. J. C*, **75** (2015) 235.
- [4] CMS COLLABORATION, CMS-PAS PFT-09-001 (2009).
- [5] CMS COLLABORATION, CMS-PAS PFT-10-001 (2010).
- [6] CDMS COLLABORATION, *Phys. Rev. Lett.*, **111** (2013) 251301.
- [7] CMS COLLABORATION, CMS-PAS EXO-15-003 (2016).
- [8] CMS COLLABORATION, CMS-PAS EXO-14-004 (2015).
- [9] FOX P. J., HARNIK R., PRIMULANDO R. and YU C.-T., *Phys. Rev. D*, **86** (2012) 015010.
- [10] BUSONI G., DE SIMONE A., MORGANTE E. and RIOTTO A., *Phys. Lett. B*, **728** (2012) 412.
- [11] BUSONI G. *et al.*, *JCAP*, **06** (2014) 060.
- [12] BUSONI G. *et al.*, *JCAP*, **09** (2014) 022.
- [13] CMS COLLABORATION, CMS-PAS EXO-12-047 (2014).
- [14] CMS COLLABORATION, CMS-PAS EXO-12-054 (2015).
- [15] CMS COLLABORATION, *Phys. Rev. D*, **91** (2015) 092005.
- [16] CMS COLLABORATION, *JHEP*, **06** (2015) 121.
- [17] CMS COLLABORATION, CMS-PAS EXO-15-007 (2016).
- [18] CMS COLLABORATION, CMS-PAS EXO-14-012 (2015).
- [19] CMS COLLABORATION, CMS-PAS EXO-15-010 (2016).
- [20] CMS COLLABORATION, *Eur. Phys. J. C*, **75** (2015) 151.
- [21] CMS COLLABORATION, *Phys. Rev. D*, **91** (2015) 052012.